Combined use of space-borne SAR interferometric techniques and ground-based measurements on a 0.3 km2 subsidence phenomenon

Daniel Raucoules, Charles Cartannaz, Francis Mathieu, Dominique Midot

Combined use of space-borne SAR interferometric techniques and ground-based measurements on a 0.3 km^2 subsidence phenomenon

D. Raucoules[a]*, C. Cartannaz[b], F. Mathieu [a], D. Midot[b]

[a] *BRGM, 3 avenue Guillemin, 45060, Orléans, France*

[b] *BGRM Lorraine, 1 avenue du parc de Brabois, 54 500, Vandœuvre-lès-Nancy.*

**corresponding author: d.raucoules@brgm.fr*

Highlights:

- DInSAR is applied to a subsidence phenomenon covering a small area (0.3 km²).
- A combination of conventional DInSAR using L-Band data and PSI technique is proposed.
- The results were used for adapting a ground-based network to the deformation characteristics.

Abstract:

The built-up area of the village Hilsprich (Lorraine, France) is affected by a subsidence phenomenon localized over a few hundred square metres, causing damage to buildings. In this study, differential SAR interferometry (DInSAR) was used to:

- estimate the boundaries of the subsidence in order to optimize ground-based monitoring networks (levelling and geophysical measurements)
- estimate the maximum deformation and highlight the evolution of the phenomenon (previously unknown due to insufficient historical ground-based data).

The study was based both on L-band ALOS/PALSAR SAR data and C-band Envisat/ASAR data. The interest in PALSAR data lies in its better performance for InSAR with respect to C-band data on the affected non-urban areas (such as fields and farmlands) where, in addition, conventional techniques such as topographical survey information was limited, and had often not been carried out before the first damage was observed. Conventional DInSAR based on PALSAR data processing for the 2008–2010 period identified the boundary of the subsidence area and estimated its maximum magnitude. The PSI technique in the ASAR archive gave information regarding the beginning of the subsidence. The precision of the DInSAR results was consistent with

the topographical data (in locations where this information was known) and therefore favours the SAR interferometric techniques in this context. Combined with the knowledge of the regional geological and structural setting, together with results from ground-based electrosounding, the results of the study established a basis for an increased understanding of the subsidence phenomenon, which was revealed to affect an elliptical bowl-shaped area due to salt dissolution.

Keywords: Differential SAR interferometry; salt dissolution-induced subsidence; ALOS data

1. Introduction

The village of Hilsprich (Lorraine, France) is affected by subsidence whose origin was unclear even in 2010 (Cartannaz, 2009), but which is now believed to be related to a salt dissolution phenomenon (Mathieu, 2011). Building damage was first observed in 2006. Survey levelling monitoring points have been installed and regularly revisited since October 2008 along the streets of the village, particularly in the vicinity of the damaged buildings.

The purpose of the present study was to provide maps of the ground surface deformation using space-borne differential interferometric synthetic aperture radar (DInSAR). The first objective was to delineate the affected area more precisely than is possible by levelling, using interferometric synthetic aperture radar (InSAR), which produces image-based results, then estimate the deformation rates as well as the date of the beginning of the phenomenon. The second objective was to optimise the distribution of the measurements by improving the levelling network and the geophysical profiles positions, in order to correctly define the whole affected area. Finally, combined with the other information, using the DInSAR results to improve our understanding of this phenomenon and its future evolution.

Two limitations to the application of InSAR lie on the characteristics of the subsidence bowl. The first limitation is related to the expected deformation rates and bowl size. The maximum deformation is more than 5 cm/yr over a relatively small area of about 1 km x 300 m. Such a large deformation gradient might limit the use of large time spans (e.g. Raucoules et al., 2007), and could also reduce the effectiveness of techniques similar to persistent scatterer interferometry (PSI) that are known to underestimate high deformation rates because of temporal unwrapping issues (e.g. Raucoules et al., 2009). The second limitation is the temporal decorrelation

phenomenon (Zebker and Villasenor, 1992) that would affect the non-urban part of the affected area. C-band data is known to be much less effective than L-band over agricultural or vegetated areas, and PSI techniques generally obtain very low persistent scatterer densities (Ferretti et al., 2003) because of the lack of long-term targets in that type of land cover.

Considering this context, the following strategy was applied:

(1) Map the deformation using data from the Advanced Land Observing Satellite phased array L-band synthetic aperture radar (ALOS/PALSAR) to establish the boundary of the subsiding bowl and estimate the maximum deformation rates. Although the precision was expected to be relatively low (≈ 1 cm/yr, by combining small temporal baseline PALSAR interferograms) it was considered adequate for the high deformation rates in this case.

(2) Use of C-band data (Envisat ASAR) to compute a PSI times-series on persistent scatterers (PS) near the boundary of the subsidence. We therefore expected to observe small deformations for these points at the margin of the stable area, but the process would nevertheless provide information regarding the temporal evolution of the deformation.

Combining these two approaches was expected to contribute to the objectives of the study; it should be noted that the strategy was constrained by the small amount of available data for the period of interest. Had we had access to a dense archive of PALSAR images prior to 2006 (e.g. tens of images instead of a total of eight), the second approach would not have been needed: PSI based on PALSAR data would have provided the required information.

2. SAR Interferometry methodology

Space-borne DInSAR is widely used for obtaining ground surface deformation caused by earthquakes (e.g. Massonnet, 1993), urban subsidence due to water pumping (e.g. Raucoules et al., 2003), landslides (e.g. Delacourt et al., 2009) or mining subsidence (e.g. Perski & Jura, 1999; Gueguen et al., 2009). Its capabilities and limitations are well known (e.g. Massonnet & Feigl, 1998; Zebker & Villasenor, 1992; Hanssen, 2001). The present case, however, involved partially vegetated land cover and high deformation gradients (i.e. high

deformation rates across a small subsidence width), for which L-band data was considered to be the best choice (e.g. as discussed in Raucoules et al., 2007).

Therefore, the first approach based on L-band data was the following. After acquiring all available L-band data (PALSAR) for the test site and for the period of interest, all possible interferograms were then produced. The most reliable interferograms were selected visually, following Le Mouélic et al. (2005). The selection was based on the apparent phase noise and on the similarities between the deformation signatures on the interferograms (deformation signature is assumed to be similar for the different interferograms, whereas atmospheric effects differ). Selected interferograms were therefore unwrapped. Since the deformation signatures corresponded to less than one fringe, unwrapping errors are not likely to occur. The unwrapped interferograms were then stacked to increase the ratio between the deformation signal and the different errors (particularly atmospheric effects and unwrapping error). The result is a map of deformation rate in cm/yr. In this case, however, the small PALSAR dataset for the site (eight images, as mentioned) during the deformation period prevented us from determining the evolution of the deformation by this first approach.

Therefore, the second approach was aimed at applying PSI (e.g. Ferretti et al., 2001; Werner et al., 2003) on targets in the vicinity of the subsidence bowl, based on a series of Envisat/ASAR data. We expected that these points would be capable of reflecting the temporal evolution of the deformation but with much smaller amplitude than points located near places of maximum deformation. Noteworthy is the fact that the strong and irregular deformation rates appeared to be a limitation for standard PSI applications (Raucoules et al., 2009); therefore the proposed approach was also to take this into account. In addition, PSI techniques are generally inefficient outside urban or unvegetated areas because of the few scatterers that are stable for the whole period of data acquisition.

Both approaches were applied using GAMMA/IPTA software (GAMMA-RS ^{TM}).

3. Remote Sensing data

The following sections describe the SAR data used for this study.

3.1 ALOS PALSAR data

The objective was to select the largest available PALSAR dataset for the study site, keeping in mind that we preferred to produce interferograms with short temporal baselines, for the reason that we were not constrained to obtain very high precision. We anticipated high deformation rates that could be identified even with low precisions of, say, several cm/yr, but we nevertheless needed to avoid large time spans to reduce the significant temporal decorrelation effects that occur with agricultural ground cover.

We acquired two series of four PALSAR images, which was the complete single-polarisation PALSAR images set for the site. Because of the different orbits of the two tracks (series 647 and 648), it was not possible to produce interferograms between them. Our dataset allowed the production of only two series, each of six interferograms. Combining interferograms from different series is only possible once the interferograms are geocoded.

Table 1. ALOS/PALSAR acquisitions

Series 1 (track 647)	Series 2 (track 648)
28 Feb 2007	02 Feb 2008
16 Jan 2008	19 March 2008
17 April 2008	23 Dec 2009
21 Jan 2010	25 March 2010

Mean incidence angle: 38°

3.2 Envisat data set

We acquired 38 Envisat/ASAR images for the test site spanning the period from 2004 to 2009. The objective was to provide information on the temporal evolution of the phenomenon, in particular its commencement in 2006. Images were acquired in mode I2 on track 337.

Table 2: Envisat/ASAR acquisitions

Year	Acquisitions dates
2004	22 Jan, 26 Feb, 1 April, 10 June, 15 Jul, 19 Aug
2005	06 Jan, 10 Feb, 21 April, 26 May, 30 June, 04 Aug, 08 Sept, 13 Oct, 17 Nov, 22 Dec
2006	26 Jan, 02 March, 11 May, 15 June, 20 Jul, 24 Aug, 28 Sept, 02 Nov, 07 Dec
2007	11 Jan, 15 Feb , 22 March, 26 April, 31 May, 05 July
2008	10 April, 02 Oct, 11 Dec
2009	19 Feb, 04 June, 17 Sept, 26 Nov

Mean incidence angle: 23°

4. Observations

Figure 1 shows the location of the affected area. Before the present study, most of the subsidence deformation had been observed in the built-up section of the village. Figure 2 shows the three ALOS interferograms that were considered to be the more relevant for our purpose, after visual selection. The subsidence phenomenon was localized in a consistent way on the interferograms. However, some discrepancies were evident (locally up to 1 rad), which could have been due to atmospheric interference, as mentioned previously, but were probably also caused by variations in the soil characteristics (L-band signals are more affected than C-band by a thick upper soil layer, and the phase value is more highly influenced by variables such as humidity). Finally, the observed deformation signature was smaller by about a quarter of a fringe; we were therefore at the limit of the sensitivity of the technique based on individual interferograms. For these reasons, interferogram stacking was required to improve the result. However, although the various possible sources of detection errors were reduced, they could not be ignored since they were of the same order as the deformation signatures themselves, and interpretation based on the expected location and characteristics of the deformation (shape

and simililarity between interferograms) could not be avoided. The aim of the study was not to detect new deformation signatures, but to better characterise the previously observed subsidence; thus the constraints of location, subsidence rates and so on made the interpretation more straightforward.

Line-of-sight (LOS) displacements were converted in subsidence rates from the three interferograms, assuming no horizontal component of displacement. From this information, a mean deformation map was derived for the period February 2008 – March 2010 (Figure 3).

Our assumption that horizontal deformation did not contribute to the LOS measurements invites further examination. Subsidence is generally associated with horizontal displacement: for example, Tandanand and Powell (1991) showed that, for coal mining subsidence, the maximum horizontal displacement is about 20–40% of the maximum vertical displacement. However:

(1) Even at a 38° angle of incidence (ASAR data), the SAR geometry is less sensitive to the cross-track horizontal component than to the vertical component. If the ratio of horizontal/vertical displacement is 30%, the contribution to LOS of the horizontal cross-track motion is about 23% of the vertical. An along-track horizontal component does not affect the InSAR measurement.

(2) For a subsidence bowl, the horizontal displacement at the center of the bowl is not the maximum displacement; this occurs at the inflexion points of the cross-section of the bowl. Thus the estimated maximum vertical displacement is little affected by the horizontal component of displacement.

The main information gained from the measurements was therefore the outline, or boundary, of the subsidence area (previously unknown) and the maximum deformation rate (about 9 cm/yr vertically).

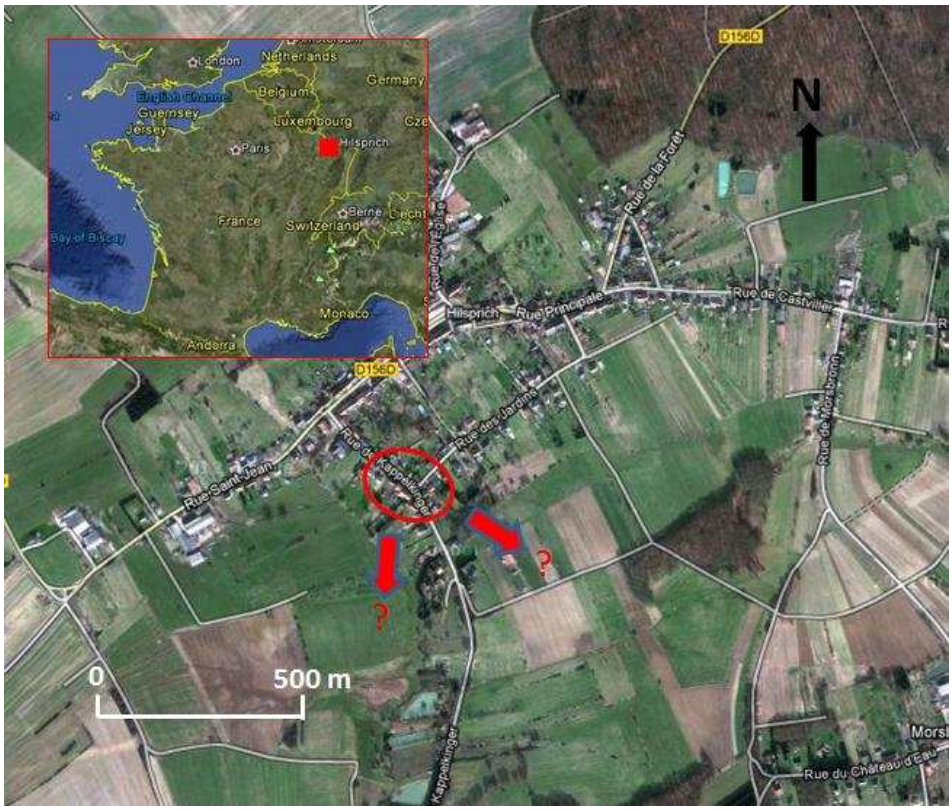

157

158

159 Figure 1. Location of test site. The red ellipse is the area with observed subsidence effects on buildings in 2008. One of the
160 purposes of the InSAR application was to investigate the actual extent of the deformation (in particular in the directions
161 represented by the arrows).

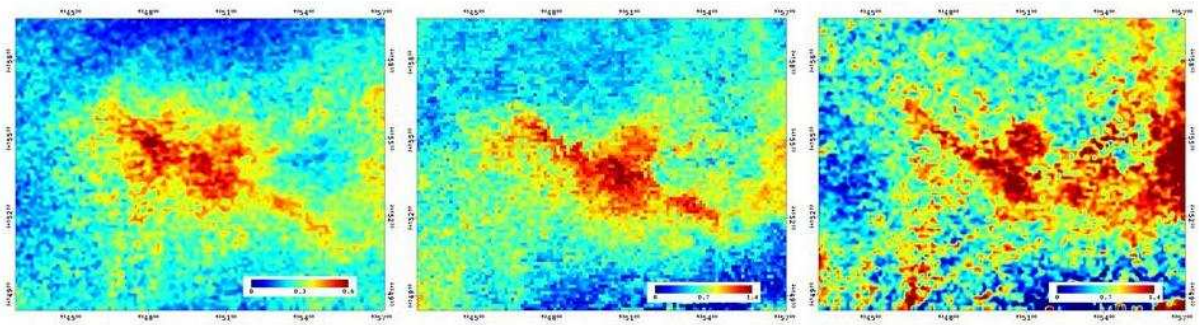

162

163

164 Figure 2. The three most relevant ALOS/PALSAR interferograms (values in radians); Lambert II étendu projection (metres).

165

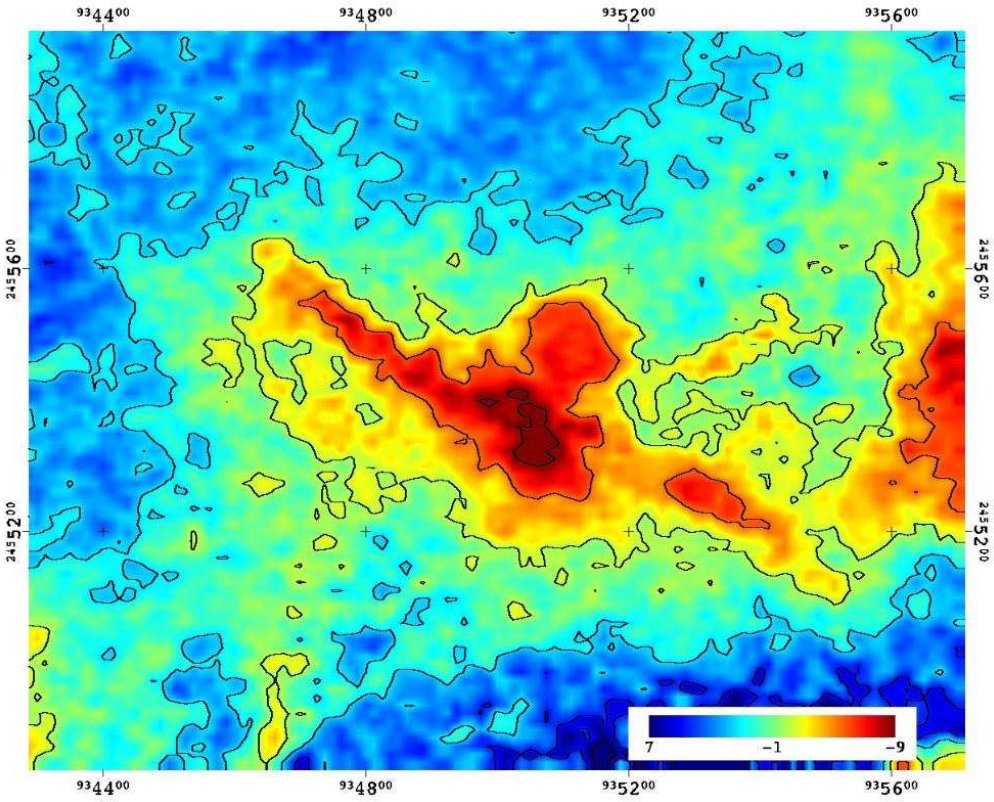

Figure 3. Stacked unwrapped interferograms from Figure 2 (values in cm/yr for line-of-sight (LOS) displacement). The zero was fixed arbitrarily to correspond to what we assumed to be stable areas. Contour interval 3 cm/yr; Lambert II étendu projection (metres). For the 38° incidence angle, 3 cm/yr along LOS corresponds to 3.8 cm/yr vertical displacement.

An additional observation concerns the rate variation: the comparison of two interferograms (Figure 4) shows a slight apparent decrease (about 30%) in the maximum rate of subsidence between 2008 and 2010. This observation, based as it is on a comparison between only two interferograms, does not imply with certainty that the rate was decreasing; since we were dealing with a complex phenomenon, deformation could be irregular, comprising periods of slower and faster movement. However, recently surveyed levels (2012) confirmed that the rate had decreased globally in the previous four years, as detailed in Figure 9.

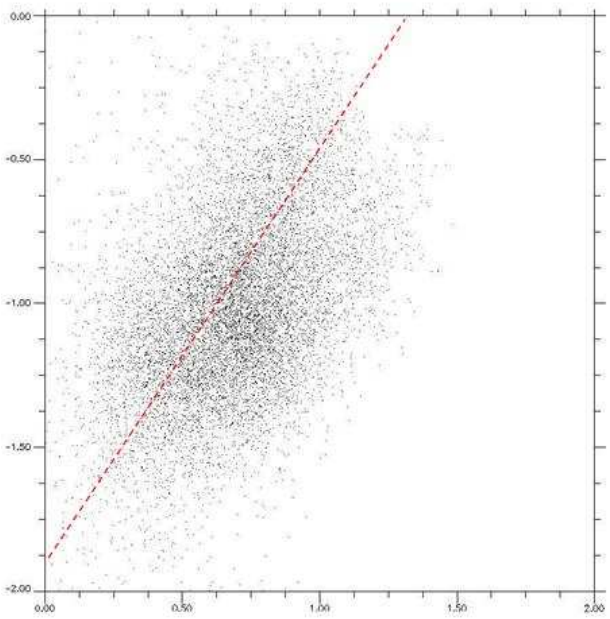

Figure 4. Scatter plot of interferograms. X-axis = phase (radians) of interferogram 23/12/2009 – 25/03/2010 for a sector centered on the subsiding area; Y-axis = phase of interferogram 16/01/2008 – 14/04/2008. Slope of line of best fit (red broken line) corresponds to a rate ratio for 2010:2008 of about 0.7.

The results of PSI processing shown in Figures 5–8 represent the evolution of selected PS slightly affected by subsidence. PS close to the subsiding area, but whose time series appears stable, are not shown. PS in the area considered as the most affected by subsidence were rejected by the algorithm during processing. The two PS we considered to be the most relevant for interpretation are shown in Figure 6, which is the average. The other four time series are shown in Figure 8. Although the evolution before and after 2006 is not obvious (the ramp on the time series before 2006 was refuted by the partial PSI analysis shown in Figure 6, and is probably a consequence of phase unwrapping issues in 2008 due to the reduced amount of data for that period), the major subsidence event that occurred in 2006 is clearly seen, as corroborated by inhabitants of the town who spoke of obvious increased surface deformation and damage at that time. The observed PS moved some 1 to 1.5 cm between May and July 2006, a period of less than three months.

It should be noted that the located PS were at the boundary of the subsidence bowl that had been estimated from data acquired in 2008. This does not prevent the possibility of previous, slower, deformation closer to the centre of the bowl.

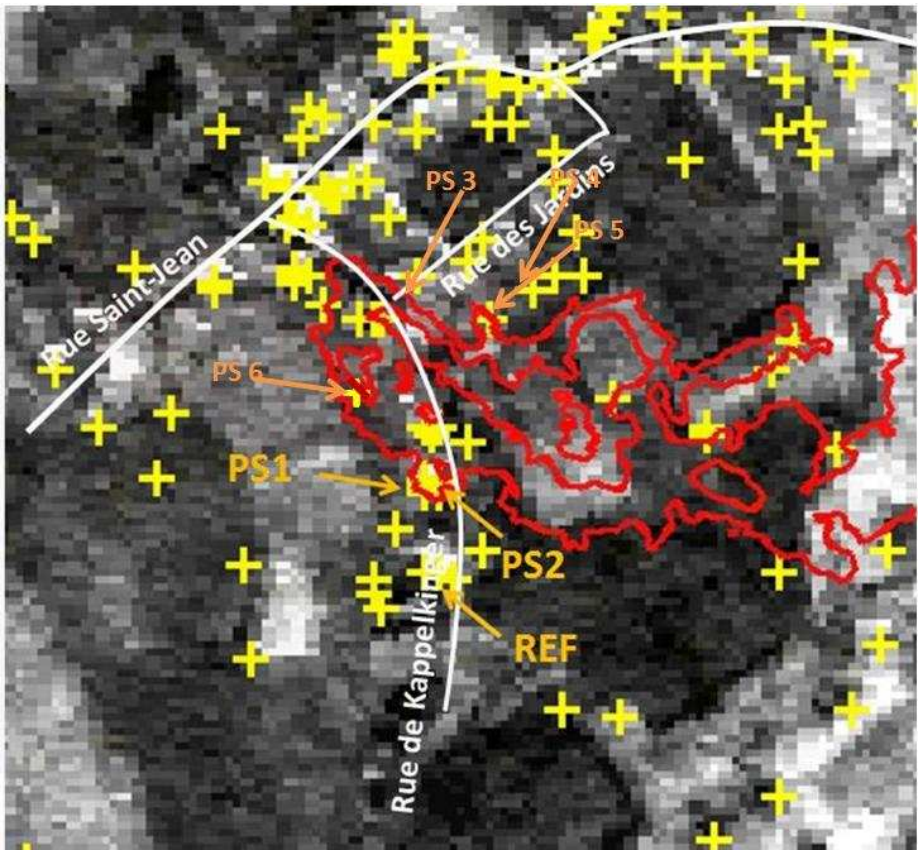

195

196 Figure 5. Location of the investigated PS (in yellow). PS of special interest (close to the deformation boundary)

197 and the chosen reference are shown.

198

199

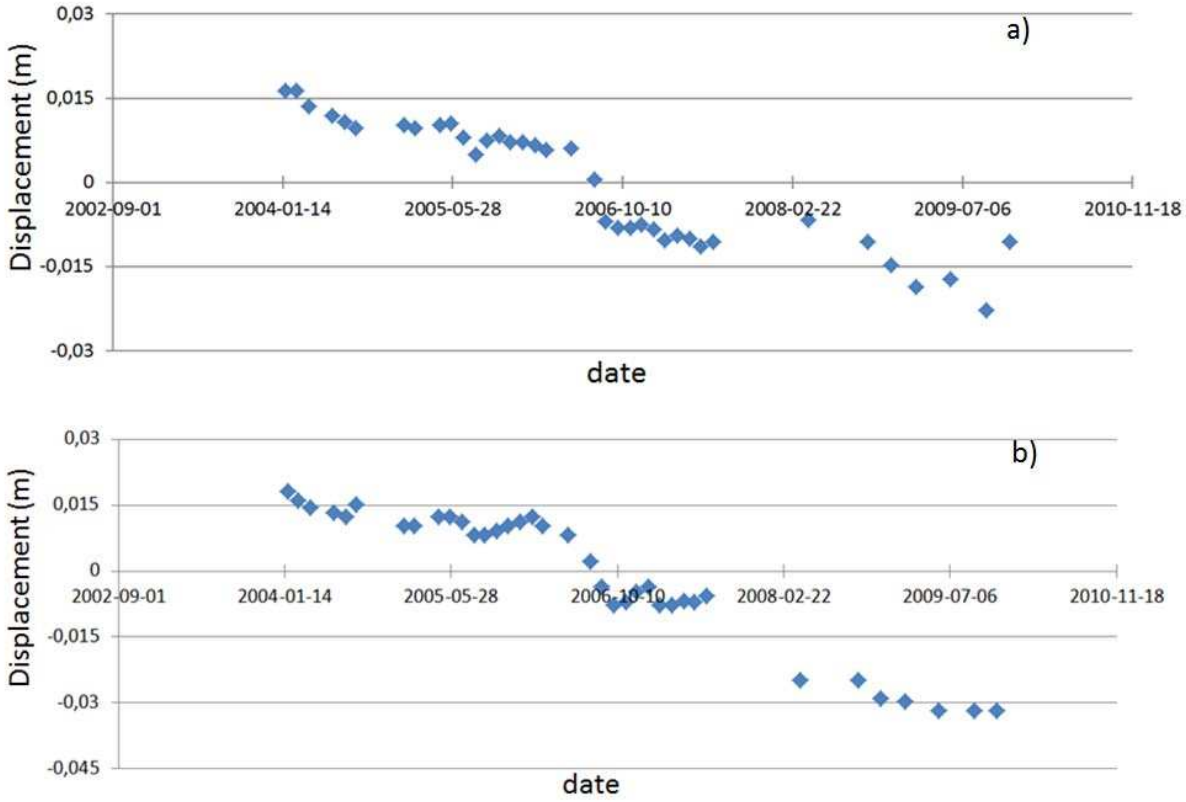

200

201 Figure 6. Time series of the PS showed in Figure 4: (a) PS1; (b) PS2. The 2006 event is clear on the time series. The trend
202 before 2006 could be due to temporal unwrapping issues. In particular, note the lack of information for 2007 and 2008,
203 resulting in apparent phase jumps, and hampering the completeness of the record for this period. The mean subsidence
204 rate derived from these time series is about 6.2 mm/yr.

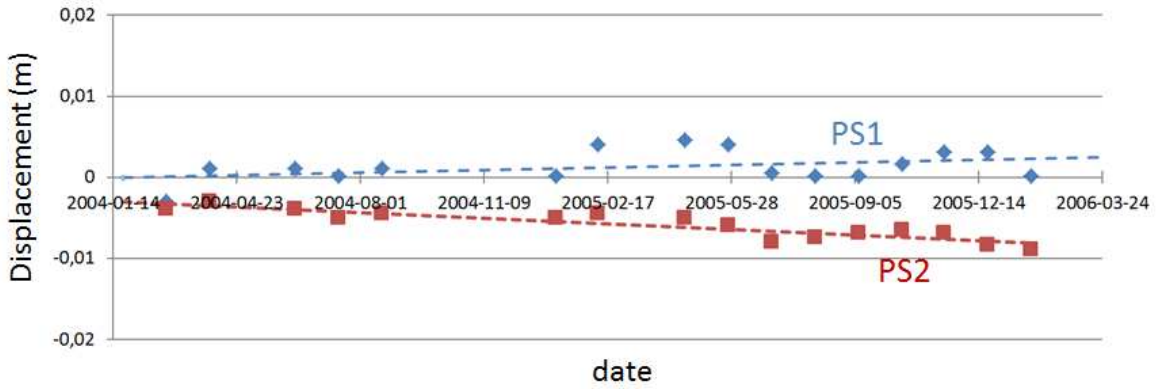

205

206

Figure 7. Time series of the PS shown in Figure 4, based only on images acquired before 2006. These show that the previously observed trend (in particular for PS1) is a processing bias and therefore the PS can be considered to be stable. Note that processing was based on 16 images only, and was therefore less precise than if more data was available.

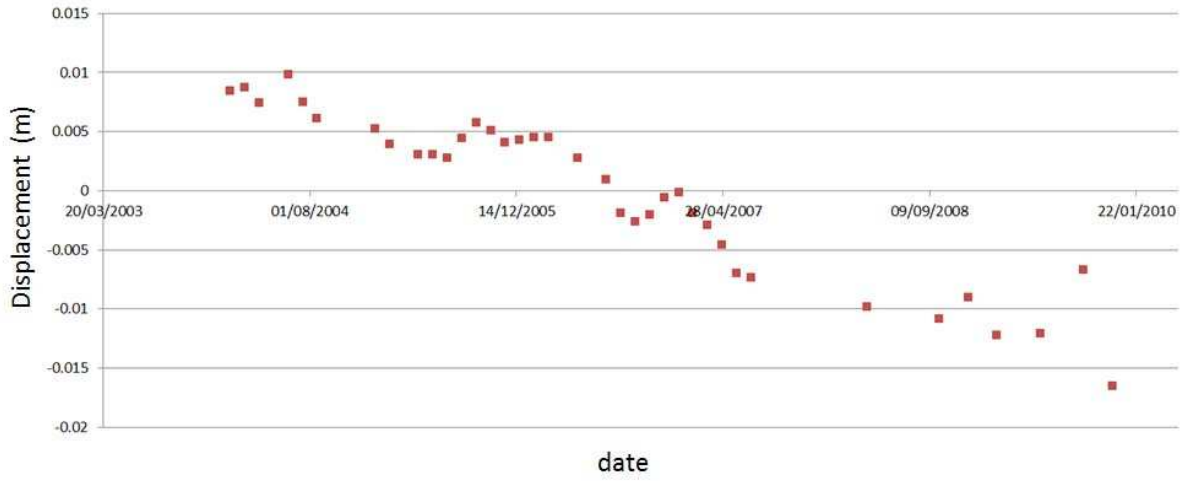

Figure 8. Average of the time series for PS 3–6. The more rapid deformation indicated for May–July 2006 was confirmed to average 7 mm at those four points. The overall mean rate derived from this time series is about 4 mm/yr.

5. Optimisation of measurement and monitoring networks

Improved mapping of the subsidence location allowed us to (1) adjust the levelling-based monitoring network, and (2) define a strategy for implementing the electrical measurement profiles (detailed in Mathieu, 2011).

Figure 9 shows the positions of points in the modified levelling network. The intention was to focus the observations on the relevant areas; note in Figure 9 the levelling points added near Brendel, which confirmed the InSAR-based observations that deformation was mainly localized south-east of the first observations (Figure 1) and pointed out a possible south-easterly acceleration and/or migration of the phenomenon. Future evolution on this area should therefore be regularly monitored.

Figure 10 shows the mean evolution in an area situated near the junction of rue Kappelkinger and rue des Jardins. These levelling points had been monitored since 2008 (and are different from points in the network modified in 2011). It is notable that the levelling time series possibly indicates different behaviours, and that

the standard deviation is about 3 cm/yr for the estimated mean value on each date. If it is confirmed that the deformation rate decreased by about 30% between 2008 and 2010, as suggested by Figure 4, the rate fluctuated in 2008. In addition, DInSAR apparently underestimated the values at the monitored levelling points, indicating a vertical displacement rate of about 7–8 cm/yr compared to about 11–12 cm/yr by levelling for the same period. Several hypotheses can be combined for explaining this discrepancy: (1) The inaccuracy of the chosen reference stable area. This choice was partly arbitrary; in addition, the interferometric phase value can be influenced by local effects (e.g. atmospheric lengthening) that could alter the whole of the estimated deformation. (2) A possible smoothing effect of the filter applied to reduce the noise level, thus lowering the higher values. (3) More generally, the overall precision of surface displacement based on three interferograms spanning less than three months (45 to 91 days). If we assume that, at the scale of the studied area, each interferogram was affected by an imprecision of about 1 cm—a typical value for an atmospheric phase screen fluctuation (Raucoules et al., 2007)—then, after stacking and conversion, an inaccuracy in the deformation rates of about 2–3 cm/yr can be expected.

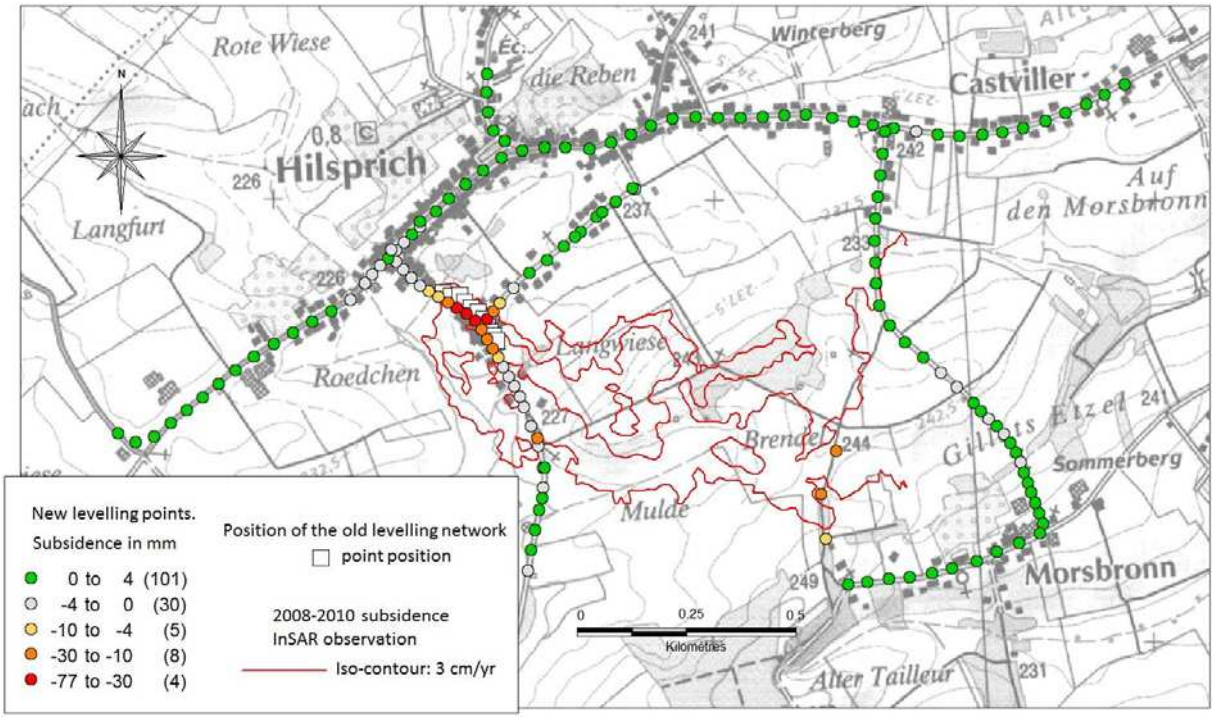

Figure 9. Modified levelling network and subsidence values (simplified 3 cm/yr isopleths) for 27/10/2011 – 17/09/2012. White squares represent the original monitoring network (source Cartannaz & Midot, 2011).

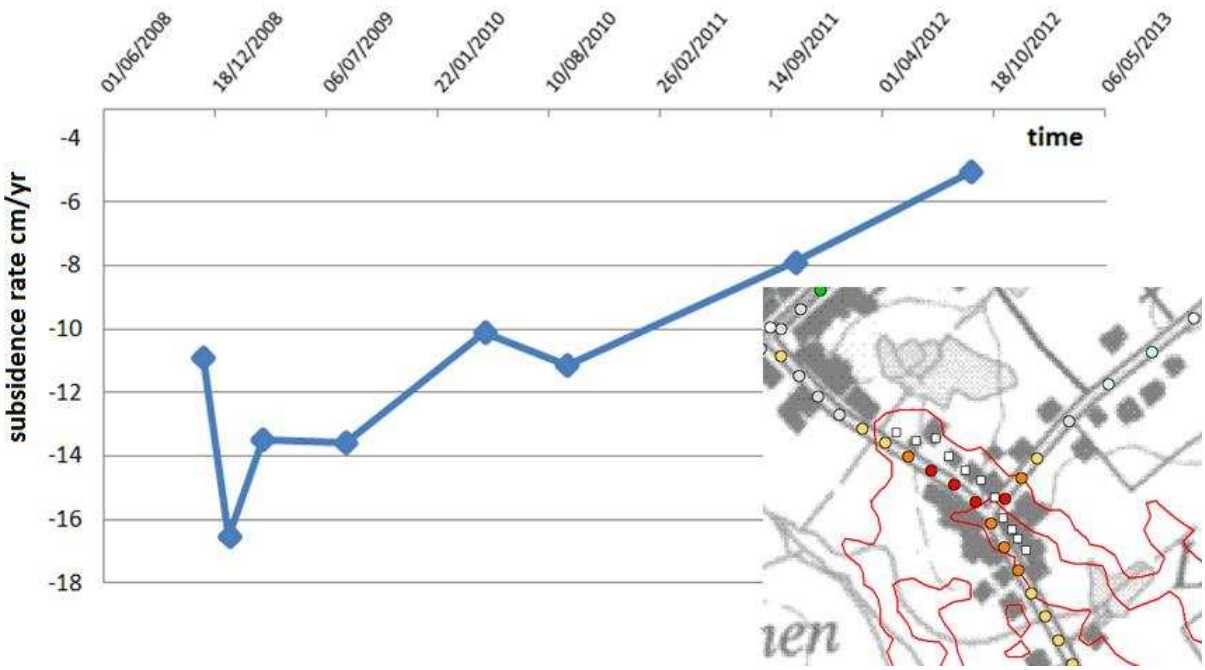

242

243

244 Figure 10. Average time series of nine levelling points located where indicated by the

245 white squares on the inset (extract from Figure 8).

246 ## 6. Discussion and Conclusion

247 The present study addressed the subsidence phenomenon in Hilsprich, in which SAR interferometric techniques
248 provided useful information. Conventional DInSAR based on PALSAR data processing for the 2008–2010 period
249 revealed clear boundaries for the subsidence area, an elliptic bowl 1 km long × 0.3 km wide, and estimated the
250 maximum subsidence rate to be about 9 cm/yr. It also seems to show a possible decrease of the rate.
251 Application of the PSI technique using ASAR data indicated that the subsidence began to occur in June 2006.

252 The limitations for such an exercise were: (1) The small PALSAR dataset limited the possibility of interferogram
253 stacking for enhancing the ratio between the deformation signal and various sources of signal degradation
254 (atmospheric effects, etc.) (2) The temporal decorrelation of non-built-up areas required the use of short
255 temporal baselines. Since this limited the reliability of the results for slow deformation rates, we were
256 constrained to focus on more rapid deformation rates of several cm/yr.

257 The major methodological interests of the study were to demonstrate the applicability of simple DInSAR
258 processing of a reduced set of ALOS/PALSAR data (eight items only) on subsidence of small lateral dimension in

non-urban sectors, and the use of this information to install a consistent, on-site, ground-based monitoring system for optimizing the measurement networks. Electrical auscultation devices were localized on the basis of these observations and the levelling network was redefined.

Finally, it points to the applicability of future L-band missions, such as ALOS-2, that appear to be adapted to this kind of phenomenon/land-cover context. In terms of risk management related to subsidence, phenomena with similar characteristics (rate, size, environmental context) in fact occur relatively frequently.

Acknowledgements:

This study was carried out with the support of a French fund for major natural hazards prevention ("Barnier Fund"). We thank the Territory of Moselle departmental directorate for collecting this fund with the aim of hazard mapping in Hilsprich.

References

Cartannaz, C. (2009*). Avis sur le diagnostic géotechnique du CETE de l'Est à Hilprich (57), Lorraine - Rapport BRGM/RP-57858-FR*. Orléans : BRGM

Cartannaz, C., & Midot, D. (2011*). Audit des levers topographiques sur la commune d'Hilsprich - Rapport BRGM/RP-60100-FR*, Orléans: BRGM

Delacourt, C., Raucoules, D., Le Mouelic, S., Carnec, C., Feurer, D., Allemand, P., & Cruchet, M. (2009). Observation of a large scale landslide in La Reunion Island using Differential SAR interferometry (JERS and Radarsat) and correlation of optical images (Spot 5), *Sensors*, 9(1):616–630.

Ferretti, A., Prati, C., & Rocca, F. (2001). Permanent scatterers in SAR interferometry, *IEEE Transactions on Geoscience and Remote Sensing*, 39(1):8–20

Ferretti A., Colesanti, C., Perissin D., Prati C., & Rocca, F. (2003). Evaluating the effect of the observation time on the districution of SAR Permanent scatterers, *Proceedings of the Fringe 2003 Workshop*, Frascati: ESA (pp. 1–5)

285 Guéguen, Y., Deffontaines, B., Fruneau, B., Al Heib, M., De Michele, M., Raucoules D., Guise, Y., & Planchenault, J. (2009).
286 Monitoring residual mining subsidence of Nord/Pas-de-Calais coal basin from Differential and Persistent Scatterer
287 Interferometry (Northern France, *Journal of Applied Geophysics,* 69(1):24–34

288 Hanssen, R. F. (2001). Radar Interferometry: Data Interpretation and Error Analysis, Dordrecht: Springer Verlag.

289 Le Mouélic S., Raucoules D., Carnec C., & King C. (2005). A least-squares adjustment of multi-temporal InSAR data –
290 Application to the ground deformation of Paris, *Photogrammetric Engineering and Remote Sensing*, 71,(2):197-204
291 Massonnet, D., Rossi, M., Carmona, C., Adragna, F., Peltzer, G., Feig,l K., & Rabaute, T.(1993). The displacement field of the
292 landers earthquake mapped by radar interferometry, *Nature*, 364:138–142
293
294 Massonnet, D., & Feigl, K. (1998). Radar interferometry and its application to changes in the Earth's surface. *Review of.*
295 *Geophysics,* 36(4):441
296
297 Mathieu, F. (2011). *Caractérisation d'un affaissement par méthodes électriques sur la commune d'Hilsprich (57) - BRGM/RP-*
298 *60482-FR*, Orléans: BRGM

299 Perski, Z., & Jura, D. (1999). ERS SAR interferometry for land subsidence detection in coal mining areas, *Earth Observation*
300 *Quarterly*, 63:25–29

301 Raucoules, D., Colesanti, C., & Carnec, C. (2007). Use of SAR interferometry for detecting and assessing ground subsidence,
302 *Compte Rendus Geosciences*, 339(5):289

303 Raucoules, D., Le Mouélic, S., Carnec, C., Maisons, C., & King C. (2003). Urban subsidence in the city of Prato (Italy)
304 monitored by radar satellite radar interferometry, *International Journal of Remote Sensing*, 24(4):891

305 Raucoules, D., Bourgine, B., de Michele, M., Le Cozannet, G., Closset, L., Bremmer, C., Veldkamp, H., Tragheim, D., Bateson,
306 L., Crosetto, M., Agudo, M., & Engdahl, M. (2009). Validation and intercomparison of Persistent Scatterers Interferometry:
307 PSIC4 project results, *Journal of Applied Geophysics*, 68(3):335–347.

308 Tandanand, S., & Powell, R. (1991). Determining horizontal displacement and strain due to subsidence, Washington D.C:
309 U.S. Dept. of the Interior, Bureau of Mines

310 Werner, C., Wegmuller, U., Strozzi T., & Wiesmann, A. (2003). Interferometric point target analysis for deformation
311 mapping. *Proceedings of IGARS'03*, Toulouse: Geoscience and Remote Sensing Society, 7:4362–4364

312 Zebker, H.A, & Villasenor, J. (1992). Decorrelation in interferometric radar echoes, *IEEE Transactions on Geoscience and*
313 *Remote Sensing*, 30:950–959.